LAWRENCE
LIVERMORE
NATIONAL
LABORATORY

UCRL-JRNL-223013

MODELING OF NI-CR-MO BASED ALLOYS: PART II - KINETICS

P. E. A. Turchi, L. Kaufman, Z.-K. Liu

July 20, 2006

CALPHAD

Updated October 14, 2003

Modeling of Ni-Cr-Mo based alloys: Part II – kinetics

P. E. A. Turchi[a], L. Kaufman[b], and Zi-Kui Liu[c]

[a]Lawrence Livermore National Laboratory (L-372), P. O. Box 808, Livermore, CA 94551, USA

[b]140 Clark Road, Brookline, MA 02445-5848, USA

[c]Department of Materials Science and Engineering, 209 Steidle Building, The Pennsylvania State University, University Park, PA 16803, USA

Abstract

The CALPHAD approach is applied to kinetic studies of phase transformations and aging of prototypes of Ni-Cr-Mo-based alloys selected for waste disposal canisters in the Yucca Mountain Project (YMP). Based on a previous study on alloy stability for several candidate alloys, the thermodynamic driving forces together with a newly developed mobility database have been used to analyze diffusion-controlled transformations in these Ni-based alloys. Results on precipitation of the Ni_2Cr-ordered phase in Ni-Cr and Ni-Cr-Mo alloys, and of the complex P- and σ-phases in a surrogate of Alloy 22 are presented, and the output from the modeling are compared with experimental data on aging.

1. Introduction

In Part I, several aspects of the statics of phase formation and transformation in Ni-Cr-Mo-based alloys, including Alloy 22 selected for the Yucca Mountain Project (YMP), have been presented together with the thermodynamic database that has been adapted for this series of alloys [1]. The current design assumes that radioactive waste will be deposited at the proposed Yucca Mountain site in waste disposal canisters that may have the surrounding space between canisters filled with another material to slow down or prevent the possible seepage of waste into the local environment. These waste disposal canisters must survive local environmental conditions as well as conditions exacerbated by the radioactive waste itself. The YMP requires that the design and manufacture of the waste containment system that will prevent the leakage of nuclear waste into the environment must be stable over a period of 100,000 years. Hence, to design these waste canisters, decisions

must be made as to the materials the canister should be manufactured from as well as the construction and design of the canisters. Kinetics studies of phase transformations in these alloys constitute one critical aspect in the selection process. In particular, the formation of the oP6 ordered phase (of Ni_2Cr-type, or $C11_b$) and of the Frank-Kasper or tcp (tetrahedrally close-packed) phases (in particular σ and P) over long time must be examined. Indeed on one hand, the ordering transformation that takes place in these Ni-Cr-Mo-based alloys has been linked to an increased susceptibility to stress corrosion cracking (SCC) and hydrogen embrittlement. Hence, it is of great relevance to predict the rate at which long-range order is occurring in Alloy 22 under repository conditions. On the other hand, the Frank-Kasper phases P, μ, and σ are present in the weld metal in the as-welded condition. These phases are known to cause embrittlement, especially at grain boundaries where their nucleation starts. Although it may be possible to eliminate these phases through heat treatment, this may be difficult for the closure weld since the spent-nuclear-fuel cladding cannot be heated to more than 350 °C. These analyses will determine if the precipitation that occurs during the welding process has a significant effect on weld properties. If the weld properties are found to be adequate, it will be determined whether aging of Alloy 22 welds causes the precipitates to change in such a way that the properties are affected.

To achieve these goals, and since these phase formations are diffusion controlled, the DICTRA (Diffusion Controlled TRAnsformation) application software [2,3] is well suited for these studies. In section 2 diffusion modeling is briefly presented. Then, in section 3, a modification of the mobility database is presented to account for available experimental data on the binary Ni-Cr alloy and the formation of an oP6 ordered phase from the face-centered cubic (fcc, or A1) matrix. In section 4, the results are validated in the case of a ternary Ni-Cr-Mo alloy with results on Temperature-Time-Transformation (TTT) curve. For an additional alloy composition of the ternary alloy that represents a reasonable surrogate of Alloy 22, the TTT results are presented for the transformation from the fcc matrix to the oP6 ordered phase. In section 5, the TTT results of the fcc to P and fcc to σ transformations are discussed for this surrogate ternary system. Finally, conclusions are drawn in section 6.

2. Diffusion modeling of phase transformations

Process simulations require the development of a kinetic description of alloy systems, *i.e.*, the knowledge of the mobility of the species in individual phases [4-6]. The models that relate the mobility and diffusivity are based on the generalized Onsager flux equation. As an example, for a

phase consisting of a substitutional sublattice and an interstitial sublattice, the intrinsic diffusion coefficient, D_{kj} (the diffusivity of component k with respect to the gradient of component j), is related to the atomic mobility M_i (i for all the elements in a phase) with the following formula [3,6]

$$D_{kj} = \sum_{i\in S}\left(\delta_{ik} - u_k\right)u_i M_i \frac{\partial \mu_i}{\partial u_j} + \sum_{i\notin S}\delta_{ik}u_i y_{Va} M_i \frac{\partial \mu_i}{\partial u_j} \qquad (1)$$

with $u_k = x_k \Big/ \sum_{i\in S} x_i$ and $\delta_{ik} = \begin{cases} 1 & i=k \\ 0 & i\neq k \end{cases}$

where $i\in S$ denotes that component i is substitutional and $i\notin S$ interstitial. x_k is the mole fraction of component k. μ_i is the chemical potential of component i derived from the Gibbs energy of the phase. The variable y_{Va} represents the site fraction of vacancy in the interstitial sublattice. The mobility M_i associated with species i is further related to a frequency factor M_i^0 and composition by the following equations [3,6]

$$M_i = \frac{1}{RT}\exp\left(\frac{\Delta G_i}{RT}\right) \qquad (2)$$

$$\Delta G_i = \sum_j \sum_m y_j^{I} y_m^{II} \Delta G_i^{j:m} + \sum_j \sum_{k>j} \sum_m y_j^{I} y_k^{I} y_m^{II} \Delta G_i^{j,k:m} + \sum_j \sum_n \sum_{m>n} y_j^{I} y_n^{II} y_m^{II} \Delta G_i^{j:n,m} \qquad (3)$$

where ΔG_i is the activation Gibbs energy of component i, and $\Delta G_i^{j:m}$ the activation Gibbs energy of component i with components j and m on the first and second sublattices, respectively. The interaction terms $\Delta G_i^{j,k:m}$ and $\Delta G_i^{j:n,m}$ are expressed with a polynomial similar to the summations in Eq. (5) in Part I [1]. The individual parameters are evaluated from chemical and tracer diffusion data.

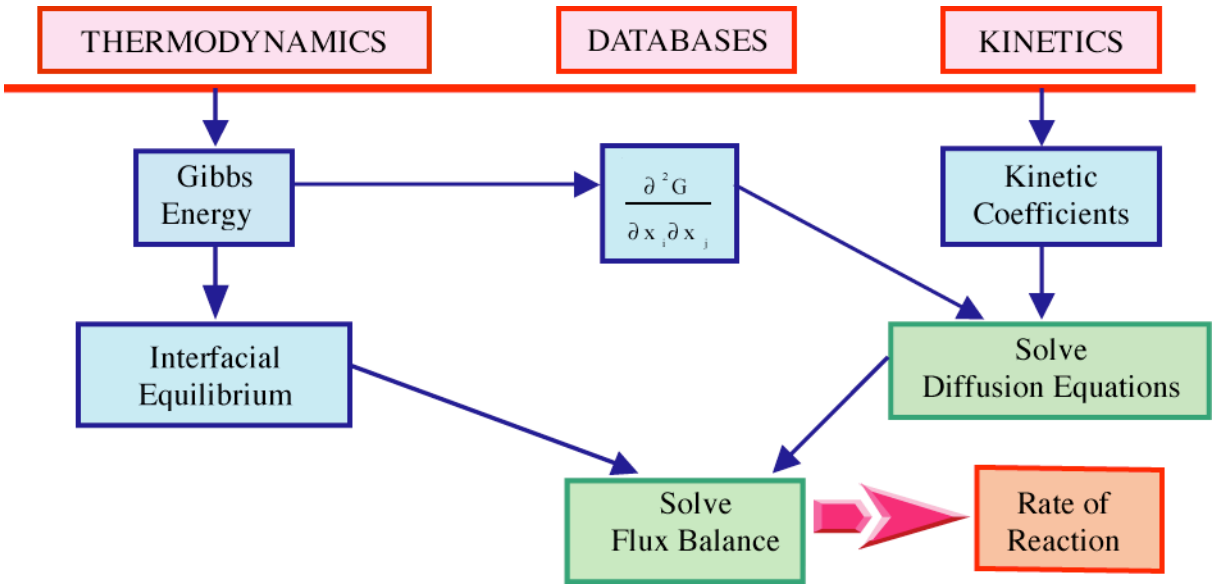

Figure 1. (Color online) Schematic flow chart for the numerical simulation of the kinetics of phase transformations.

By combining the thermodynamic and kinetic descriptions of alloy systems, phase transformations can then be simulated. The schematic flow chart of the DICTRA simulation is recalled in Fig. 1. The most significant feature of this simulation procedure is the coupling of thermodynamics and kinetics.

Starting with the thermo-chemical database provided by SGTE, a detailed analysis of the stability of the binary alloys Ni-Cr, Ni-Mo, and Mo-Cr, and of the ternary Ni-Cr-Mo alloys has been developed in Part I [1], and results were presented on the role of additional solutes such as Si, C, Co, Nb, Ta, and W on stability, ordering and precipitation in Ni-Cr-Mo-based alloys. In the present paper, kinetic and thermodynamic modeling have been combined and applied to the study of diffusion-controlled transformations with the use of the DICTRA software linked with Thermo-Calc. The overall approach is summarized in the schematic flow chart presented in Fig. 2 of Ref. [1].

DICTRA fulfills the need to provide critical modeling and analysis of data by solving the diffusion equations, calculating thermodynamic equilibrium (with Thermo-Calc, solving the flux-balance equations, and finally by predicting the displacement of phase-interface positions (cf. Figure 1). This application is used to analyze the kinetics of phase evolution in alloys selected for the barriers of the canisters used for storage of nuclear waste by predicting TTT (Temperature-Time-Transformation) diagrams for relevant phases forming as functions of time. In a near future this applications will help determining the effect of welding, *i.e.*, transformations under non-

isothermal conditions, and eventually post-annealing, on stability and long-term aging of selected alloys. Kinetics studies are focusing on the time-dependent formation of complex Frank-Kasper phases (such as P- and σ-phases), and on the long-range ordering in terms of phase evolution from the face centered cubic (fcc) matrix with time up to 100,000 years. All the following results are based on the use of the C22R2m.TDB thermodynamic database presented in Ref. [1] and a modified version of the MOB database called nicrt2mob.TDB.

3. Kinetic Database and phase transformation in Ni_2Cr alloy

A first series of calculations have been performed to predict the TTT curve in the case of a 10% transformation of a fcc-based Ni-Cr solid solution to the ordered Ni_2Cr (oP6) phase for which experimental data on the variation of the lattice parameter of a Ni_2Cr alloy with time at fixed isothermal annealing were available [7], see Fig. 2. By assuming that the variation of the fcc lattice parameter as a function of time is directly proportional to the amount of ordered phase formed in the disordered fcc matrix [8], three points of the TTT curve have been obtained at 450, 500, and 530 °C from Fig. 2 in the case of a 10% transformation from fcc to oP6 of the Ni-rich solid solution with 33.3 at. % Cr.

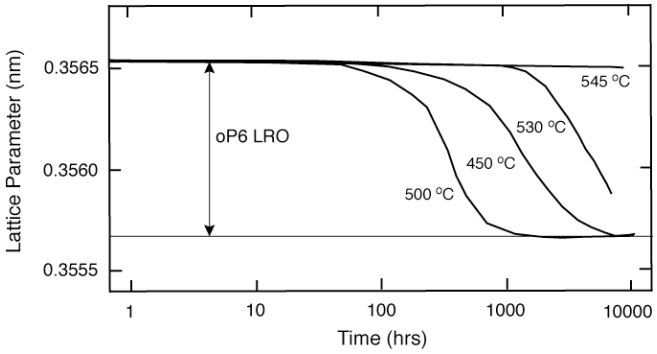

Figure 2. Experimental variation of the lattice parameter with time at fixed isothermal annealing for a Ni_2Cr alloy, redrawn from Fig. 6 of Ref. [7]. The horizontal lines delineate the range of existence of the oP6 long-range order (LRO) from the disordered phase (top line) to the

The MOB database that contains the mobility and the diffusion coefficient of the Cr species in a fcc-Ni matrix has been adjusted to account for the kinetics of transformation studied experimentally by Karmazin [7], as discussed in the following.

The property diagram of Ni_2Cr presented in Fig. 3 for the two phases, *i.e.*, the fcc-solid solution and the oP6-ordered phase, clearly indicates that the order-disorder transition temperature is about 826 K (or 553 °C), and this information will determine the asymptotic behavior in temperature of the TTT curve.

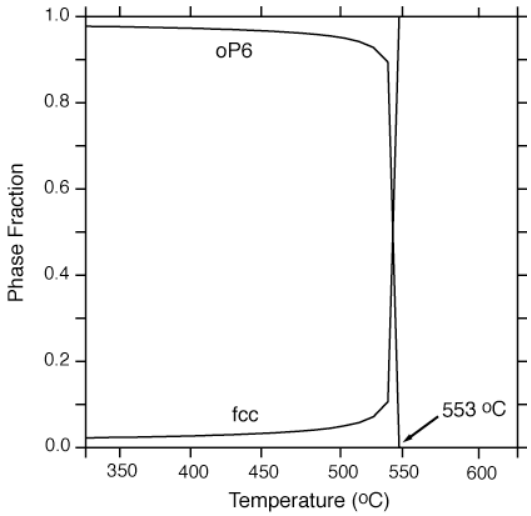

Figure 3. Property diagram of a Ni-33 at.% Cr alloy. The fcc and oP6 ordered phases are the only phases considered, and all other phases are suspended during the calculations.

The location of the nose of the experimental TTT curve has been used to determine the kinetic parameters that are defined below in the MOB database for subsequent calculations. The detailed results of the simulations for a 10% transformation are reported in the TTT curve displayed in Fig. 4. The shape of this C curve is detailed in Table 1 and by the curves displayed in Fig. 5 that show the fraction of oP6-phase formed in the fcc matrix versus time at various temperatures.

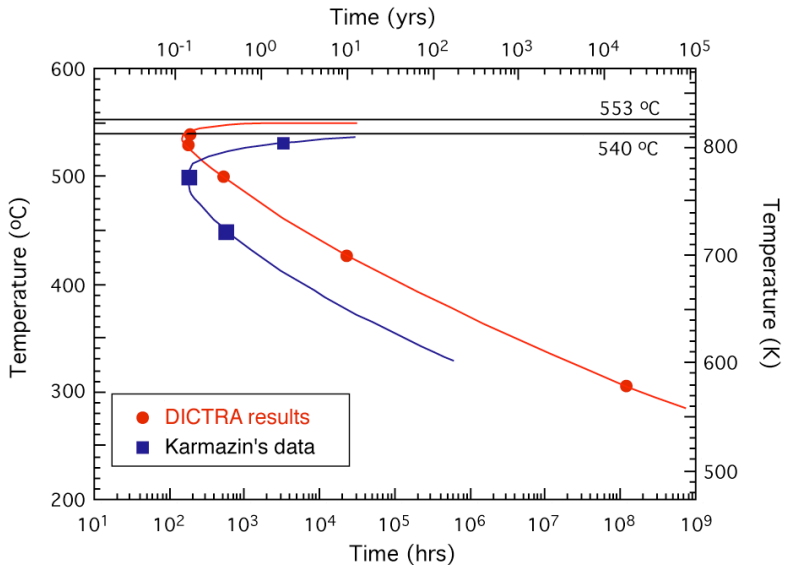

Figure 4. (Color online) Calculated Isothermal TTT diagram (solid circles) for a fcc-based matrix of a binary Ni_2Cr alloy transforming into the oP6-ordered phase, with transformation rate of 10%. The experimentally deduced TTT diagram (solid squares) [7] for the same transformation rate is also shown for comparison.

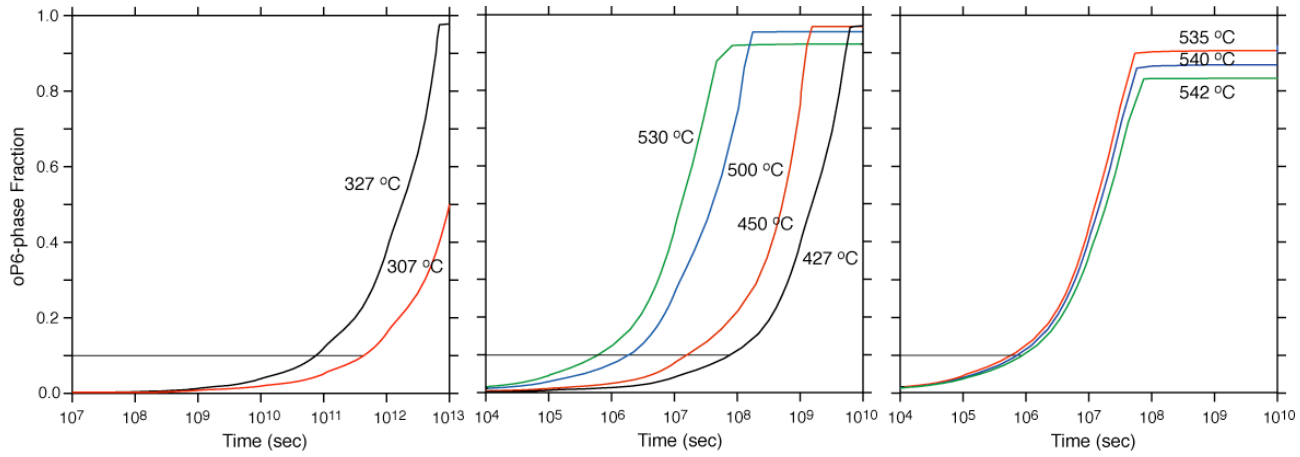

Figure 5. (Color online) Calculated phase fraction of the oP6-ordered phase formed from a fcc matrix for a Ni-33 at. % Cr alloy versus time (in sec) at various temperatures (in °C). The horizontal line indicates a 10 %-transformation from fcc to oP6.

The shape of the C curve in Fig. 4 reproduces very favorably the experimentally deduced results. From the stability studies [1] the value of the critical order-disorder temperature (that positions the asymptote in the TTT diagram), *i.e.*, 553 °C, agrees reasonably well with the experimentally assessed value of 540 °C. Note that the transformation is rather sluggish and is initiated after about 200 hours. Extrapolation of the TTT curve to lower temperatures clearly indicates that in this binary alloy the oP6-ordered phase cannot form out of the fcc-solid solution below 300 °C for as long as 100,000 years.

T (°C)	Time (hrs) 10%	Time (hrs) 10% [7]
307	117.14 10^6	
327	202.39 10^5	
427	22,064.67	
450	4,799.52	584.17
500	523.24	205.52
530	175.27	3,234.44
535	156.21	
540	185.65	
542	269.90	

Table 1. Time (in hrs) for a calculated 10%-transformation from fcc to oP6 at various temperatures for a Ni_2Cr alloy, first two columns (at left). The last column corresponds to the results deduced from experimental measurements of Ref. [7] (see also Figs. 2 and 5).

The MOB database, produced by Thermo-Calc AB, contains assessed data for the diffusion coefficients and the mobilities of concentrated alloys. Equations (4) and (5) for the fcc phase of the

Ni-Cr-Mo system display the relevant results in keeping with Eqs. (1-3) above. All phase names and thermodynamic factors are compatible with the SGTE solution database (SSOL) in J/mol.

$$\Delta G_{Cr}^{fcc} = x_{Cr}Q_{Cr}^{Cr} + x_{Mo}Q_{Cr}^{Mo} + x_{Ni}Q_{Cr}^{Ni} + x_{Cr}x_{Mo}Q_{Cr}^{Cr,Mo} + x_{Cr}x_{Ni}Q_{Cr}^{Cr,Ni}$$
$$\Delta G_{Ni}^{fcc} = x_{Cr}Q_{Ni}^{Cr} + x_{Mo}Q_{Ni}^{Mo} + x_{Ni}Q_{Ni}^{Ni} + x_{Cr}x_{Ni}Q_{Ni}^{Cr,Ni} + x_{Mo}x_{Ni}Q_{Ni}^{Mo,Ni} \quad (4)$$
$$\Delta G_{Mo}^{fcc} = x_{Cr}Q_{Mo}^{Cr} + x_{Mo}Q_{Mo}^{Mo} + x_{Ni}Q_{Mo}^{Ni} + x_{Cr}x_{Mo}Q_{Mo}^{Cr,Mo} + x_{Ni}x_{Mo}Q_{Mo}^{Ni,Mo}$$

Q_{Ni}^{Ni} =-286000-86T

Q_{Cr}^{Cr} = -286000-71.9 T

$Q_{Mo}^{Mo} = -239{,}800 + RT\ln(3.6\,10^{-6})$

Q_{Cr}^{Ni} =-287000-64.4T

Q_{Ni}^{Cr} =-235000-82T

$$Q_{Cr}^{Cr,Ni} = -68{,}000 \qquad Q_{Ni}^{Cr,Ni} = -81{,}000 \quad (5)$$

The only remaining parameter to be chosen is the cell size that represents the distance over which the solute atoms must occur during the formation of the product phase. In the original calculation [9] this distance was chosen to be 100 μm. This choice together with the validated database C22R2m.TDB database discussed in the appendix of Ref. [1], and the mobilities displayed above resulted in transformation rates that were $1x10^{-6}$ times smaller than those measured [7] and shown at 500 ºC in Fig. 2. It should be noted that the cell size also determines the number of nucleation sites per unit area (volume): the smaller the cell size the larger the number of nucleation sites. Accordingly, the mobility values indicated in Eqs. (4) and (5) were amended as shown in Eq. (6) and designated as database **nicrt2mob.TDB**.

This database in combination with the aforementioned **C22R2m.TDB** were used, together with a cell size of 100 μm, to calculate the transformations of the fcc phase to P-phase, σ-phase, and oP6. Hence the quantities given in Eq. (2) above become (in J/mol)

$$Q_{Cr}^{Cr} = Q_{Cr}^{Ni} = Q_{Ni}^{Cr} = Q_{Ni}^{Ni} = -250{,}000 \qquad Q_{Mo}^{Mo} = -239{,}800 + RT\ln(3.6\ 10^{-6})$$
$$Q_{Cr}^{Cr,Ni} = -68{,}000$$
$$Q_{Ni}^{Cr,Ni} = -81{,}000 \quad (6)$$

Note that the mobility M_i associated with species i is directly related to the tracer diffusivity by means of the Einstein relation: $D_i^* = RTM_i$. The results shown in Figs. 4 and 5 and in Table 1 have been obtained with this amended mobility database.

It is worth mentioning that Eqs. (4) and (5) can generate identical results if a cell size of 0.3 μm is used in the calculations as those derived with **nicrt2mob.TDB** and a cell size of 100 μm. The physical choice between these two sizes can be made on the basis of the following observations. First, Karmazin on pages 248 and 249 of Ref. [7] noted that the Ni-Cr ingots that he measured were ground and particles that were less than 60 μm placed in fused silica capillaries, rinsed in Argon at 200 ºC, evacuated and sealed. He concluded that the individual grains in the X-ray samples recrystallized at 1100 ºC and quenched prior to transformation consisted of independent relatively single crystals with almost free surfaces. In addition Fig. 6 shows a photomicrograph of the Wrought Alloy 22 used in recent transformation studies [9] that suggest a grain size much larger than 0.3 μm and closer to 100 μm.

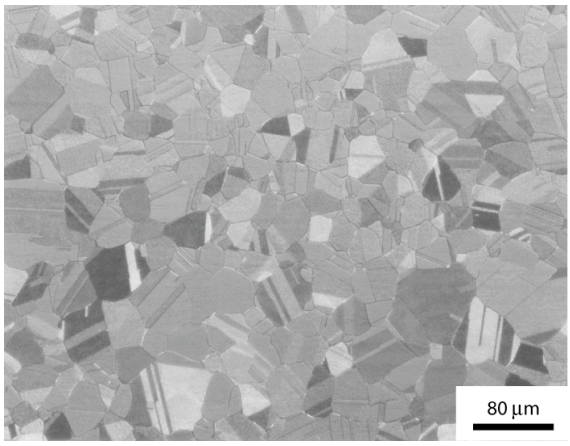

Figure 6. Microstructure of a wrought sheet of Alloy 22 [9].

4. Fcc to oP6 transformation in $Ni_x(Cr_3Mo)_{1-x}$ alloy

In this section, the results for the kinetics of transformation from a fcc matrix to the oP6-ordered phase are reported for two alloy compositions, using the ni2crt2mob.TDB database described in section 3 and a cell size of 100 μm. In the following, all compositions are in wt. % unless otherwise specified.

4.1. Fcc to oP6 transformation in a Ni-20.78 Cr-12.78 Mo alloy

This alloy composition corresponds to 24 at.% Cr-8 at.% Mo, *i.e.*, a ratio 3:1 for Cr:Mo. The property diagram of this alloy is shown in Fig. 7 and indicates that the order-disorder transition temperature is about 627 ºC.

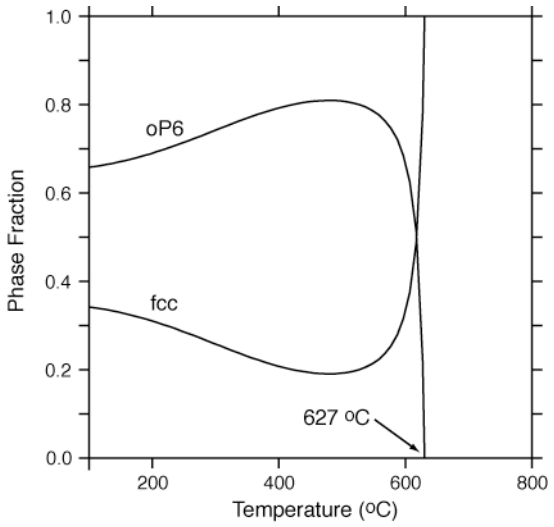

Figure 7. Property diagram of Ni-20.78 Cr-12.78 Mo (or 24 at.% Cr and 8 at.% Mo). The fcc and oP6 ordered phases are the only phases considered, and all other phases are suspended during the calculations.

The calculated kinetic results for 5, 10, and 20 % transformation from the fcc-solid solution to oP6 for Ni-20.78 Cr-12.78 Mo that are shown in Table 2 and Fig. 8 can be directly compared with those reported by Karmazin [10] in Fig. 7 of Part I [1] that have been interpreted by assuming once again that a linear relation exists between the variation of the lattice parameter and the amount of fcc matrix transformed into the oP6-oredered phase. The calculations have been performed with databases C22R2m.TDB and nicrt2mob.TDB with a cell size of 100 μm.

T (°C)	Time (hrs) 5 %	Time (hrs) 10 %	Time (hrs) 20 %
300	$444.44\ 10^6$		
400	$152.78\ 10^3$	$611.11\ 10^3$	$236.11\ 10^4$
460	3,333	$152.78\ 10^2$	$611.11\ 10^2$
560	50	208	833
580	38	142	583
600	41	169	694
615	111	472	1,944
560 [10]	23		

Table 2. Time (in hrs) for 5, 10, and 20 % transformations from fcc to oP6 at various temperatures (in °C) for a Ni-20.78 Cr-12.78 Mo alloy. The last row corresponds to the experimental result from Ref. [10].

The experimental point (solid square) at 560 °C indicated in Fig. 9 has been deduced from the experimental study of the variation of the lattice parameter with time under isothermal annealing condition [10].

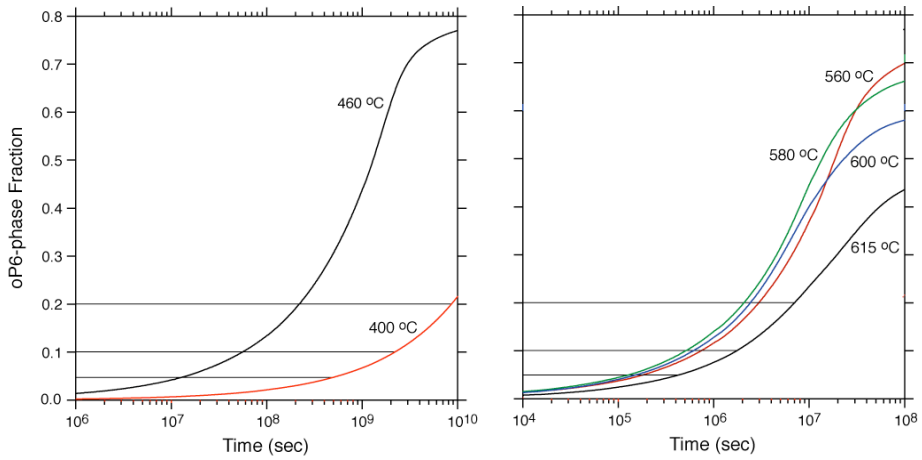

Figure 8. (Color online) Calculated phase fraction of oP6-ordered phase formed from a fcc-based matrix for a Ni-20.78 Cr-12.78 Mo alloy versus time (in sec) at various temperatures (in ºC). The horizontal lines indicate 5, 10, and 15 %-transformation from fcc to oP6.

The results displayed in Fig. 9 show that, first, the thermodynamic driving force at this alloy composition and the kinetic factors account fairly well for the kinetics of transformation, and second, although Mo enhances the stability of the ordered phase (increased critical order-disorder temperature at about 627 ºC from 553 ºC), the extrapolation of the TTT curves to lower temperatures confirms the observation already discussed in the binary case about the impossibility of forming the oP6-ordered phase out of the fcc-solid solution below 300 ºC for as long as 100,000 years.

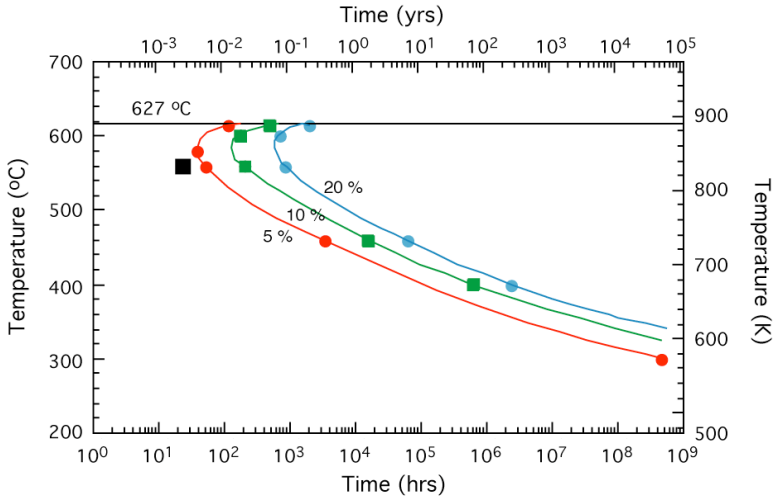

Figure 9. (Color online) Calculated isothermal TTT diagrams for a fcc-based matrix of a ternary Ni-20.78 Cr-12.78 Mo alloy transforming into the oP6-ordered phase, with transformation of 5

(red), 10 (green), and 20 (blue) %. The black solid square is the result from annealing experiments performed on a Ni-Cr-Mo alloy at the same composition [10].

4.2. Fcc to oP6 transformation in a Ni-21.1 Cr-13.5 Mo alloy

For this alloy the property diagram displayed in Fig. 10 indicates that the order-disorder transition temperature is about 627 ºC. Table 3 summarizes temperature versus time at five rates of transformation, and Fig 11 shows the details of the transformation curves as a function of temperature.

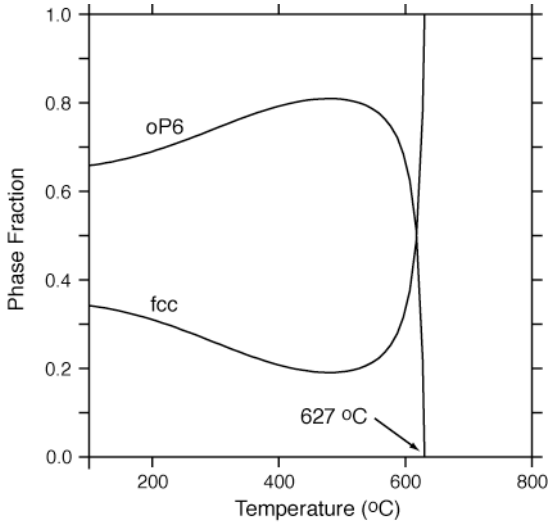

Figure 10. Property diagram of Ni-21.1 Cr-13.5 Mo. The fcc and oP6 ordered phases are the only phases considered, and all other phases are suspended during the calculations.

T (ºC)	Time (hrs) 2 %	Time (hrs) 5 %	Time (hrs) 10 %	Time (hrs) 15 %	Time (hrs) 20 %
400		$108.06\ 10^3$	$419.44\ 10^3$		$157.78\ 10^4$
460	386	2,513	9,761.47	21,910.96	39,052.21
480	133	840	3,382	7,433	12,954
500	52	306	1,157	2,621	4,695
520	19	122	488	1,067	1,868
530	13	80	323	704	1,225
600	2	14	56	122	217
610	3	19	76	168	299
625	23	130	468	1,134	2,167

Table 3. Time (in hrs) for 2, 5, 10, 15, and 20 % transformations from fcc to oP6 at various temperatures (in ºC) for a Ni-21.1 Cr-13.5 Mo alloy.

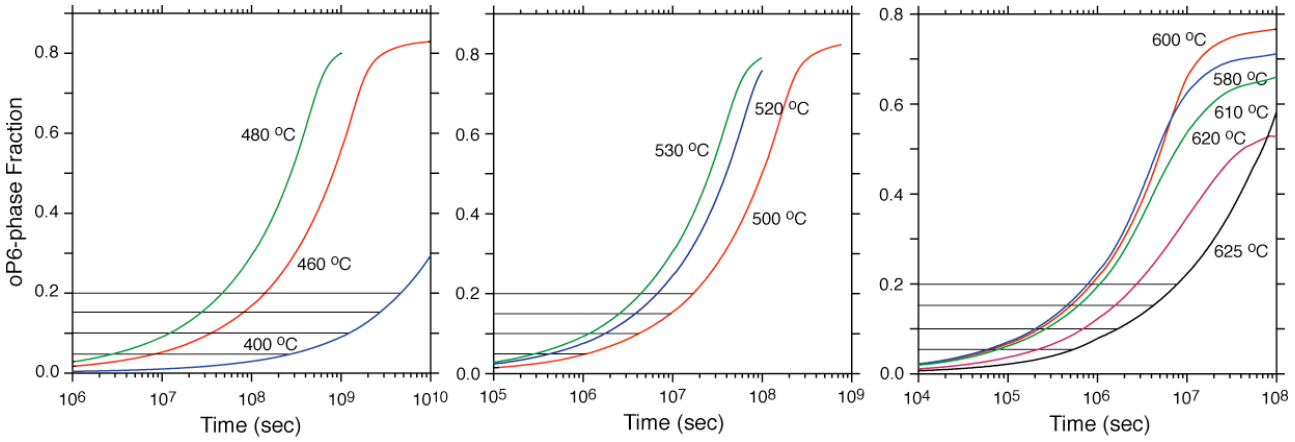

Figure 11. (Color online) Calculated phase fraction of oP6-ordered phase formed from a fcc-based matrix for a Ni-21.1 Cr-13.5 Mo alloy versus time (in sec) at various temperatures (in °C). The horizontal lines indicate 5, 10, 15, and 20 %-transformation from fcc to oP6.

Figure12 summarizes the results of the kinetics of formation of oP6 in the fcc-based matrix of the alloy at the considered composition. Note that the results are similar to those obtained for the fcc to oP6 transformation for a Ni-20.78 Cr-12.78 Mo alloy.

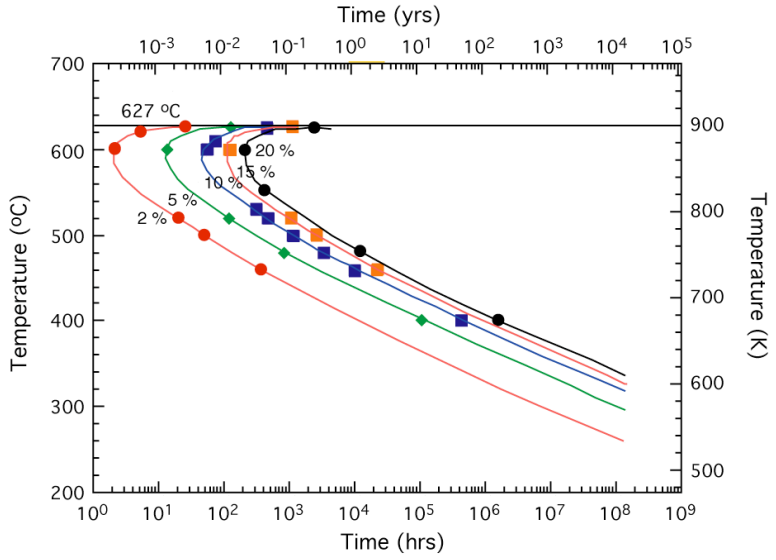

Figure 12. (Color online) Calculated isothermal TTT diagram for a fcc-based matrix of a ternary Ni-21.1 Cr-13.5 Mo alloy transforming into the oP6 ordered phase, with transformation of 2 (red), 5 (green), 10 (blue), 15 (orange), and 20 (black) %.

5. Kinetics of transformations in a surrogate of Alloy 22

For this series of calculations the case of a ternary Ni-Cr-Mo alloy is considered that can represent a surrogate of Alloy 22, with the following nominal composition: 55.7 Ni, 21.1 Cr, and 13.5 Mo. Three transformations were considered: the fcc matrix to the oP6-ordered phase, the fcc matrix to the P phase, and the fcc matrix to the σ phase. The corresponding property diagrams associated with only the fcc-based matrix and the transformed phase (oP6, P or σ) considered in the calculations are displayed in Fig. 13. Note that in the study of the kinetics of oP6-phase formation 7.5 wt.% Mo instead of 13.5 was considered. This reduction in Mo accounts for the role of W in destabilizing the ordered phase as was discussed in Part I [1]. Moreover, in all of these calculations the cell size was fixed at 100 μm and the C22R2m.TDB and nicrt2mob.TDB databases were once again used.

5.1. Fcc to oP6 transformation in a Ni-21.1 Cr-7.5 Mo alloy

In this subsection, the kinetics of transformation from a fcc matrix to the oP6-ordered phase is studied for a Ni-21.1 Cr-7.5 Mo alloy. This alloy composition accounts for the destabilizing effect of W on the oP6 –ordered phase, as discussed in section III.6 of Part1 [1]. The property diagram of this alloy is presented in Fig. 13 (left panel) and indicates that the order-disorder transition temperature is about 596 ºC. Table 4 and Fig. 14 refer to the results summarized in the TTT diagrams shown in Fig. 15.

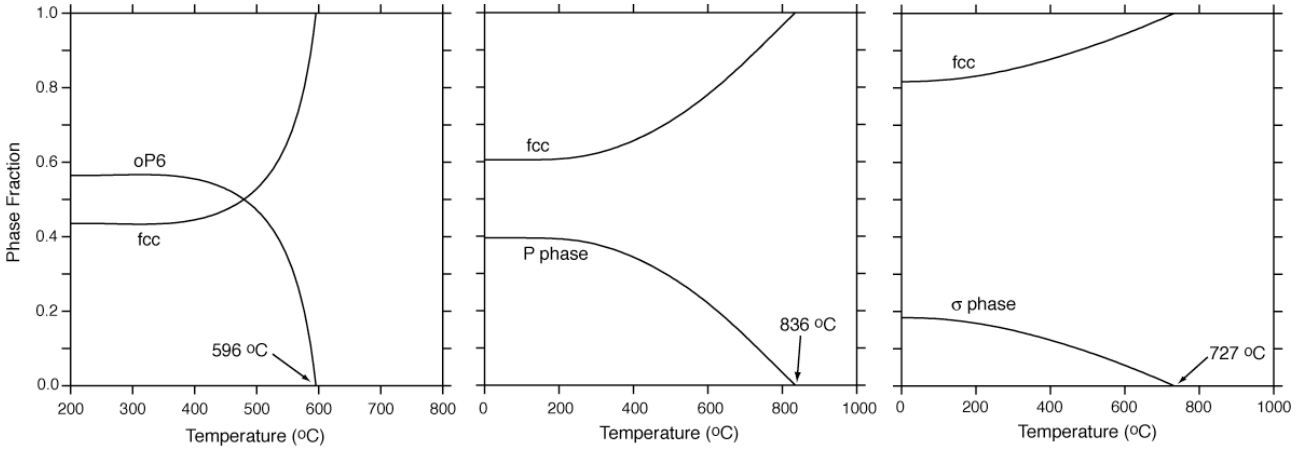

Figure 13. Property diagrams of Ni-21.1 Cr-13.5 Mo corresponding to the fcc-based matrix with the oP6-ordered phase (left panel; in this case 7.5 wt.% Mo was considered instead of 13.5; see Part I, section III.6 [1]), P phase (middle panel), and σ phase (right panel). All other phases are suspended during the calculations.

T (ºC)	Time (hrs)	Time (hrs)	Time (hrs)	Time (hrs)

	2%	5%	10%	15%
377	385.97 10^3	230.18 10^4	101.08 10^5	234.71 10^5
427	18,198	113.75 10^3	465.79 10^3	103.54 10^4
477	1,907	10,354	42,400	98,791
527	466	2,650	10,853	23,019
566	512	3,513	13,727	35,135
593	7,452	48,819.74	143.87 10^3	246.99 10^3

Table 4. Time (in hrs) for 2, 5, 10, and 15 % transformations from fcc to oP6 at various temperatures (in ºC) for a Ni-21.1 Cr-7.5 Mo alloy.

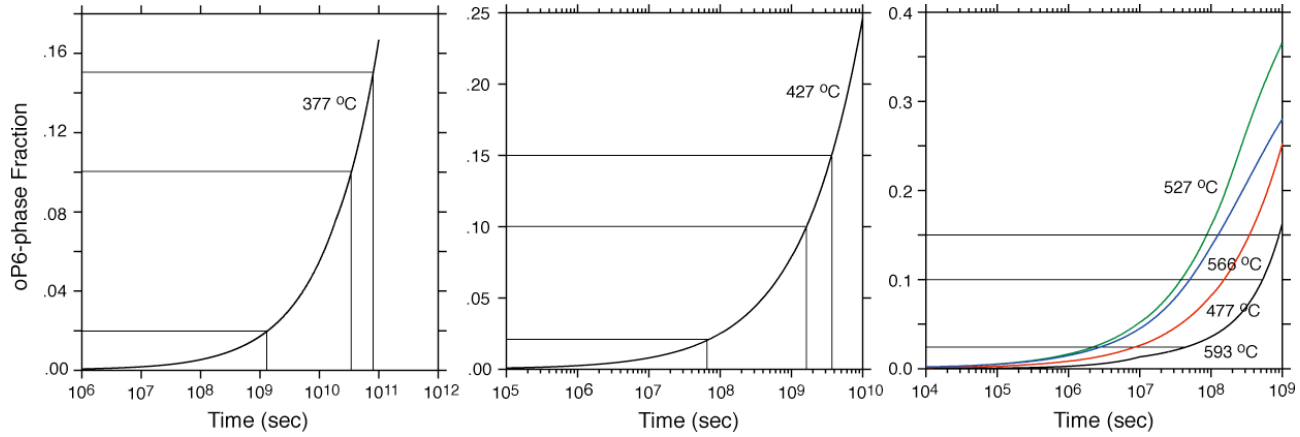

Figure 14. Calculated phase fraction of oP6-ordered phase formed from a fcc-based matrix for a Ni-21.1 Cr-7.5 Mo alloy versus time (in sec) at various temperatures (in ºC). The horizontal lines indicate 2, 10, and 15 %-transformation from fcc to oP6.

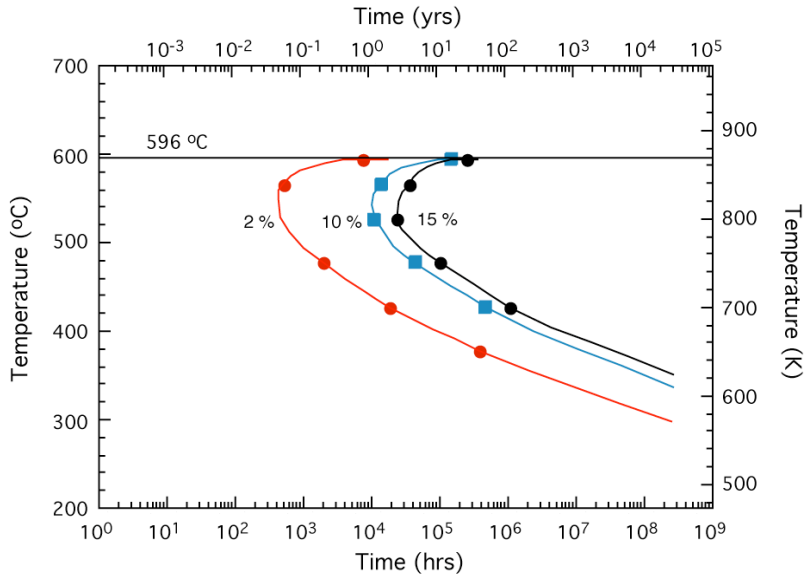

Figure 15. (Color online) Calculated isothermal TTT diagram for a fcc-based matrix of a ternary Ni-21.1 Cr-7.5 Mo alloy transforming into the oP6-ordered phase, with transformation of 2 (red), 10 (blue), and 15 (black) %.

As compared with the results for the binary Ni_2Cr alloy, the combined role of Mo and W has the effect of raising the critical order-disorder temperature from 553 to 596 ºC. Note that the TTT results are similar to those obtained for the fcc to oP6 transformation for a Ni-20.78 Cr-12.78 Mo alloy. Moreover, the reduction in the Mo content from 13.5 to 7.5 wt.% is accompanied by a reduction in the critical order-disorder temperature associated with the fcc to oP6 transformation from 627 ºC to 596 ºC, a decrease in the amount of the oP6-ordered phase formed, and a slowing down of the kinetics of the formation of the oP6-ordered phase. The reduction in the Mo composition accounts for the role played by W in Alloy 22, as discussed above.

5.2. Fcc to P-phase transformation in a Ni-21.1 Cr-13.5 Mo alloy

In this subsection, the kinetics of transformation from a fcc matrix to the P phase is studied for a Ni-21.1 Cr-13.5 Mo alloy at various temperatures. The property diagram of this alloy has been presented in Fig. 13 (middle panel) and indicates that the transformation temperature is about 836 ºC. Table 5 and Fig. 16 refer to the results that will be summarized in Fig. 18 (top figure).

T (ºC)	Time (hrs) 2%	Time (hrs) 10%	Time (hrs) 15%
427	3,365,354.61		
500	39,237.15	196,651.61	
550	3,958.62	136,774.52	303,500.24
593	948.49	27,777.78	
600	697.75	19,217.53	4,4024.81
650	163.28	3,958.62	10,486.26
700	44.02	1,289.33	
750	22.80		
760	22.06		
800	32.88		

Table 5. Time (hrs) for 2, 5, 10, and 15% transformation from fcc to P phase at various temperatures (in ºC) for a Ni-21.1 Cr-13.5 Mo alloy.

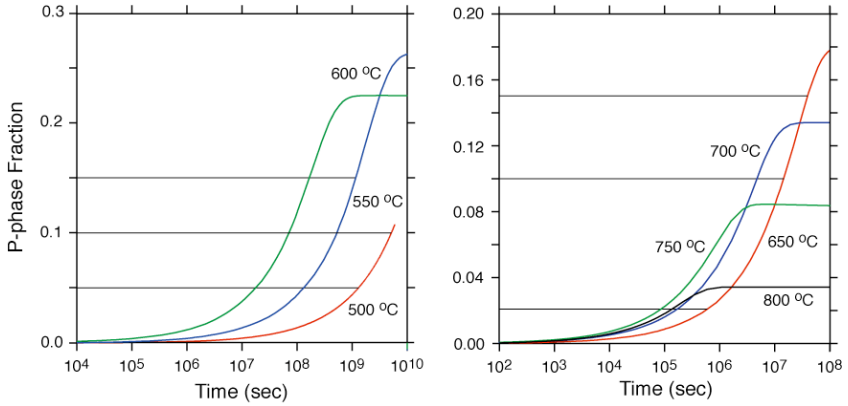

Figure 16. (Color online) Calculated phase fraction of the P phase formed from a fcc matrix for a Ni-21.1 Cr-13.5 Mo alloy versus time (in sec) at various temperatures (in ºC). The horizontal lines indicate 2, 10, and 15 %-transformation from fcc to P.

5.3. Fcc to σ-phase transformation in a Ni-21.1 wt.% Cr-13.5 wt.% Mo alloy

In this subsection, the kinetics of transformation from a fcc matrix to the σ phase is studied for a Ni-21.1 wt.% Cr-13.5 wt.% Mo alloy at various temperatures. The property diagram of this alloy has been presented in Fig. 13 (right panel) indicating that the transformation temperature is about 727 ºC. Table 6 and Fig. 17 refer to the results reported in Fig. 18 (bottom figure).

T (°C)	Time (hrs) 2 %	Time (hrs) 5 %	Time (hrs) 10 %
400	110,555,555	611,111,111	
500	361,111	2,777,777	
600	7,972	61,111	11,805,555
700	1,388	36,666	319,444
730	2,777	113,611	1,372,222

Table 6. Time (in hrs) for 2, 5, and 10 % transformations from fcc to σ at various temperatures (in ºC) for a Ni-21.1 Cr-13.5 Mo alloy.

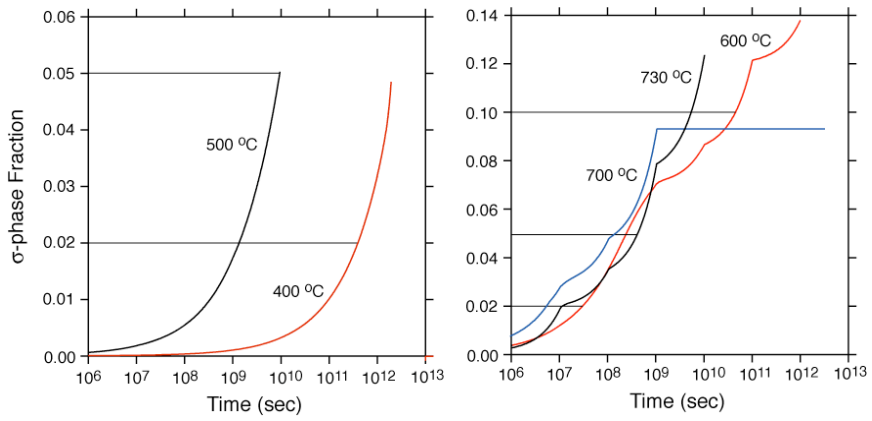

Figure 17. (Color online) Calculated phase fraction of the σ phase formed from a fcc matrix for a Ni-21.1 Cr-13.5 Mo alloy versus time (in sec) at various temperatures (in °C). The horizontal lines indicate 2, 5, and 10 %-transformation from fcc to σ.

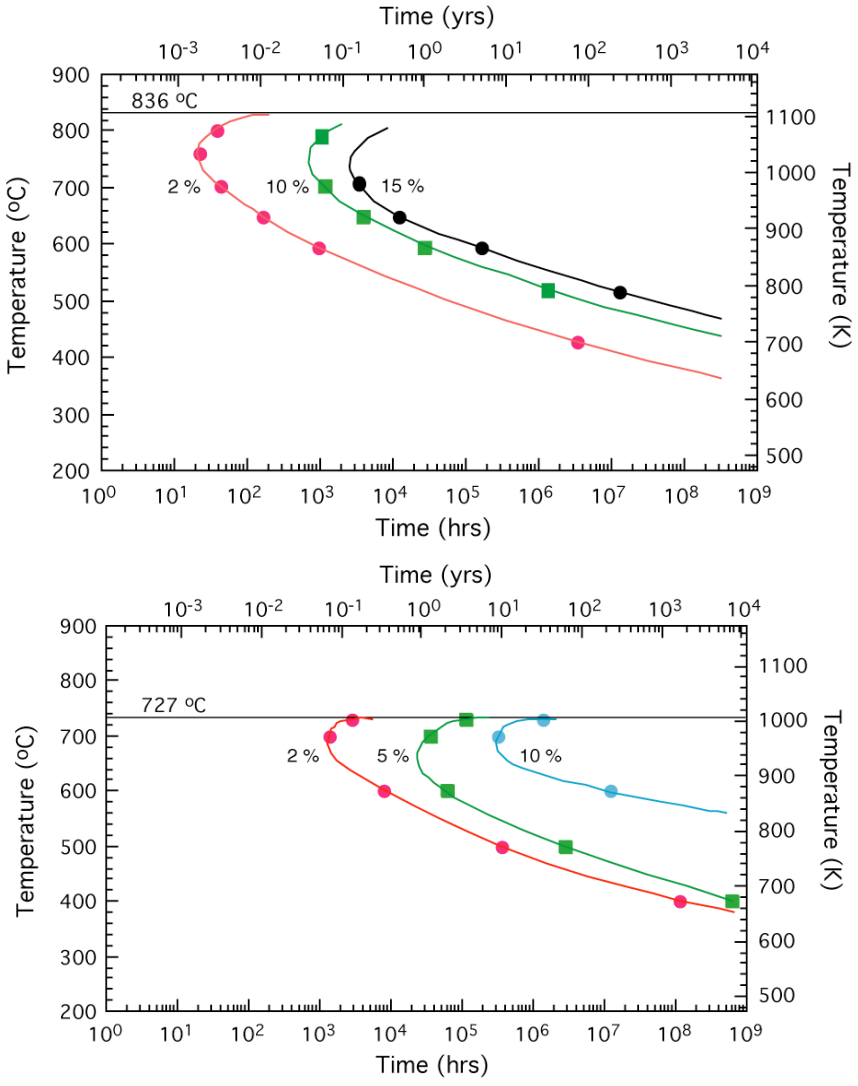

Figure 18. (Color online) Calculated Isothermal TTT diagrams for a fcc-based matrix of a ternary Ni-21.1 Cr-13.5 Mo alloy transforming into the P phase (top), and the σ phase, (bottom) with transformation rates of 2 (red), 5 (green), and 10 (blue) % for P, and 2 (red), 5 (green), and 10 (blue) % for σ phase transformations.

In Fig. 18, the TTT diagrams associated with the fcc to P, and fcc to σ transformations are displayed. The transformation from the fcc-based matrix to the P phase leads to results that are compatible with the qualitative observations performed at LLNL [11], as shown in Fig. 19. In contrast to the transformation from the fcc-matrix to the oP6-ordered phase that is rather slow, the incipient formation of the P phase is quite fast (a few hours in bulk samples). However, as was concluded, above the extrapolation of the TTT curves to lower temperatures clearly indicates the impossibility of forming the P phase from the fcc-solid solution below 300 ºC for as long as 100,000 years.

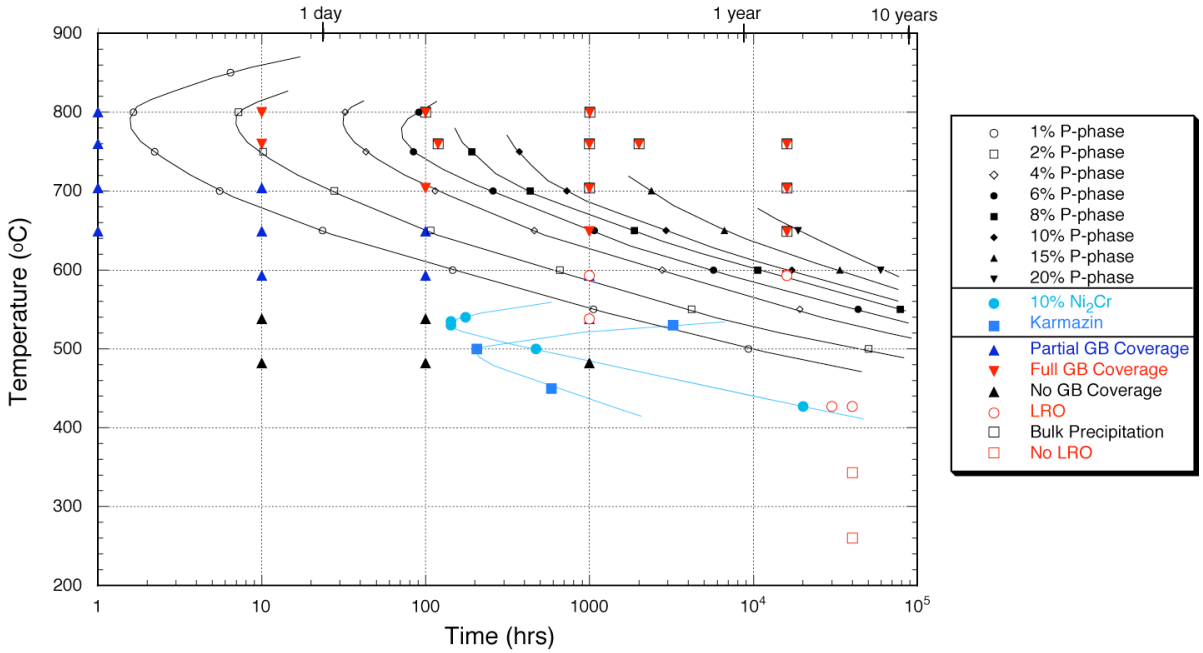

Figure 19. (Color online) Summary of the results of the isothermal TTT diagram calculated for a) a binary Ni-Cr alloy with a 10% transformation of the fcc matrix in the oP6-ordered phase of Ni_2Cr-type (lower curves describing the prediction and the results extracted from the work of Karmazin [7]), and b) a fcc-based matrix of a surrogate of Alloy 22 (*i.e.*, Ni-21.1 Cr-13.5 Mo transforming into the P phase, with transformation from 1 to 20 %.

To support the conclusions summarized in Fig. 19, Table 7 shows the results based on volume fraction measurements that were used to determine the extent of phase precipitation as function of time and temperature in Alloy 22 [12].

Temperature (°C)	Time (hrs)	% Transformation	Standard Deviation	95% Confidence Interval (%)
649	16,000	2.50	1.60	0.64
650	600	0.00	0.00	N/A
700	10,073	8.10	1.40	0.64
704	16,000	19.00	3.60	1.65
750	10,076	17.90	1.80	0.93
760	16,000	22.50	2.90	1.50
760	2,000	10.10	1.10	0.53
760	1,000	6.30	1.20	0.57
760	119	0.73	0.28	0.11
800	1,002	12.70	0.86	0.44
800	100	1.50	0.47	0.19

Table 7. Bulk precipitation area fraction measurements (% transformation) in Alloy 22 [12].

The results of phase fraction-versus-time at 700 and 750 °C for the fcc to P transformation directly obtained from simulations are reported in Fig. 20 together with those summarized in Table 7 for comparison.

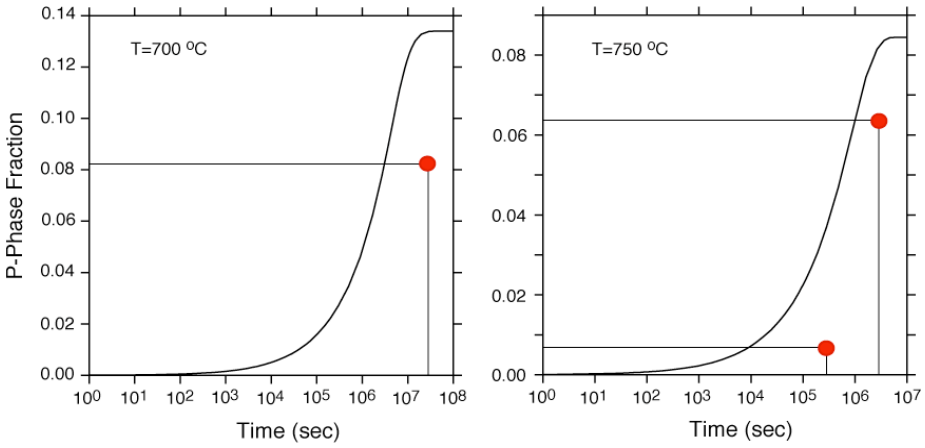

Figure 20. P-phase fraction versus time at 700 °C (left) and 750 °C (right) in Alloy 22 as obtained from simulations. The solid circles indicate the measured data [12] (see Table 7).

Kinetic calculations are performed at a given temperature and the parent and product phases have to be explicitly specified. Hence, the comparison with experiments calls for some caution. Indeed, first the volume-fraction measurements do not distinguish among the possible tcp phases (P, μ, and/or σ) that have formed, and second, the results only display one type of phase fraction at a time. As a result, Fig. 20 compares the P-phase fraction predictions with the tcp volume-fraction measurements, as the P phase is the most likely to form at these temperatures and during these times. At high temperatures and long aging times, more phases in addition to the P phase may form, which would increase ambiguity in the comparison. As a result, in order to make the comparisons as consistent as possible, only a few volume-fraction measurements from Table 7 were included. Note that according to Fig. 13 (middle panel), the maximum P-phase fraction as a function of temperature indicates that some of the results in Table 7 refer to more than a single P-phase precipitation, possibly σ at high temperatures. For example the experimentally determined volume fractions at 760 ºC on samples aged for 16,000 hrs or at 800 ºC for 1,002 hrs (see Table7) are beyond what is expected for the single P phase at these temperatures as reported in Fig. 13 (middle panel).

As noted in Fig. 20, the agreement between the simulation results and the volume-fraction measurements is satisfactory at both temperatures. The comparison shows that the computational results are conservative compared to the measured data, since the later are always located to the right (i.e., at longer time) of the simulation results. Therefore, the computational model predicts slightly earlier phase formation than what is measured at a given temperature. This conservative prediction is expected because the simulation results are based on a ternary Ni-Cr-Mo alloy, 55.7Ni-21.1Cr-13.5Mo (in wt. %), which is a surrogate for Alloy 22. Note that Alloy 22 contains less Ni (the balance of Ni will be less due to more elements specified in the actual chemical composition of Alloy 22) than the surrogate alloy considered here. Also, if others tcp phases form in Alloy 22, the kinetics of P-phase formation is expected to be slower, which is what the results reported in Fig. 20 tend to indicate.

It is worth noting that before any conclusion can be decisively drawn from this study, validation of the predictions by a quantitative analysis of phase formation in samples annealed at various temperatures and for several aging times for ternary Ni-Cr-Mo alloys that well represent Alloy 22 would be welcome. Note also, that in these calculations, phase precipitation at grain boundaries is not considered, *i.e.*, the results only apply to bulk formation and homogeneous phase evolution.

In the future, after the experimental conditions that control welding are established (composition of the filler, thermal history and temperature gradient), the DICTRA application will be used to address issues on phase formation and evolution under non-isothermal conditions in Alloy 22.

6. Conclusions

The CALPHAD methodology that has been applied to the study of the statics (stability) in Part I [1] has been extended to the study of kinetics (aging) of phase formation and evolution in Ni-based alloys. The kinetic database has been validated for the fcc to oP6 transformation in Ni-33 at.% Cr and in a pseudo-binary Ni-(Cr,Mo) alloy.

Based on these calculations it was found that the kinetics of long-range order formation occurs at relatively low temperatures, and therefore, at these temperatures, the slow diffusion process does not favor the formation of the ordered phase of Ni_2Cr-type. It is therefore very unlikely that the ordered phase will form under repository conditions, *i.e.*, below 200 °C, even for as long as 100,000 years. Finally, alloys homogenized at high temperature and quenched at relevant repository conditions should not display any deleterious phases, such as P and σ, since the kinetics of their formation is rather slow. In other words, fast cooling of Ni-Cr-Mo-based alloys annealed at high temperatures will be sufficiently efficient to avoid the precipitation of the ordered and tcp phases. Once again, it should be kept in mind that the formation of complex phases at grain boundaries usually occurs faster, and some caution is advised before drawing final conclusions based solely on the present work.

Acknowledgments

This work was performed under the auspices of the U. S. Department of Energy by the University of California Lawrence Livermore National Laboratory under Contract W-7405-ENG-48, and supported by the Yucca Mountain Site Characterization Project at LLNL. The authors are grateful to Tien Shen, Don Stevens, Bassem El-Dasher, Sharon Torres, Frank Wong, Joe Farmer, Tammy Summers, Dan McCright, and Martha Kohler for technical discussions and encouragement during the various phases of this work. ZKL would like to acknowledge the partial support from the National Science Foundation under grant DMR-0510180.

References

[1] P. E. A. Turchi, L. Kaufman, and Zi-Kui Liu, CALPHAD **30** (2006) 70-87.

[2] The Thermo-Calc and DICTRA applications software are products of Thermo-Calc AB; B. Sundman, B. Jansson, and J.-O. Andersson, CALPHAD **9** (4) (1985) 153-199; J.-O. Andersson, T. Helander, L. Höglund, Pingfang Shi, and B. Sundman, CALPHAD **26** (2), (2002) 273-312; cf. also http://www.thermocalc.com.

[3] A. Engström, L. Höglund, and J. Ågren, Metall. Mater. Trans. **25A** (1994) 1127-1134; A. Borgenstam, A. Engström, L. Höglund, and J. Ågren, J. of Phase Equil. **21** (3) (2000) 269-280.

[4] N. Saunders and A. P. Miodownik, "*CALPHAD, Calculation of Phase Diagrams: A Comprehensive Guide*", Pergamon Press (1998), 479 pages.

[5] MRS Bulletin, Vol. **24**, No. 4 (April 1999), "*Computer Simulations from Thermodynamic Data: Materials Production and Development*", p. 18-49.

[6] J. Ågren, ISIJ International **32** (1992) 291-296.

[7] L. Karmazin, Mater. Sci. and Eng. **54** (1982) 247-256.

[8] L. Kaufman, CALPHAD **25** (2006) 141-1611.

[9] B. El-Dasher, LLNL private communication (November 2005).

[10] L. Karmazin, J. Krejcí, and J. Zeman, Mater. Sci. and Eng. **A183** (1994) 103-109.

[11] T. Summers and P. Turchi, "Aging and Phase Stability of Waste Package Outer Barrier" LLNL Report No.UCRL-ID-134582 (July 1999), 115 pages.

[12] S. Torres, LLNL private communication (April 2003).